Toward a Theory of Coherent Synchrotron Radiation in Realistic Vacuum Chambers

Robert L. Warnock

SLAC National Accelerator Laboratory, Stanford University
Menlo Park, CA 94025, USA
and
Department of Mathematics and Statistics, University of New Mexico
Albuquerque, NM 87131, USA

E-mail: warnock@slac.stanford.edu

An idealized theory predicts coherent synchrotron radiation (CSR) in whispering gallery modes, in quantitative agreement with observations at NSLS-VUV in 2001. A quantitative comparison to theory was difficult for later experiments at the CLS (Canadian Light Source) owing to the complicated form of the vacuum chamber at the point of observation. Efforts to improve the theory led to a general scheme for studying fields in a rectangular chamber of varying width. It works in the frequency domain, with a spatial Fourier development only in the vertical coordinate. The calculation reduces to integration of a simple system of ordinary differential equations, with arc length s as the independent variable. A new scheme to handle a transversely singular or highly concentrated charge/current is an essential feature. If the equations are integrated by an implicit rule (trapezoidal method) the calculation can be speeded up by a large factor in comparison to explicit integration, and the paraxial approximation can be avoided, thus accommodating backward-propagating waves. The time for the field calculation is so short that it will be negligible compared to that for charge/current construction and particle pushing in a self-consistent macroparticle simulation, which could be in three dimensions.

1. Whispering Gallery Modes

Consider a beam circulating in a smooth, circular torus with rectangular cross section, with the beam centered in the cross section. The fields excited by the beam can be expressed in terms of high-order Bessel functions, since the geometry permits a separation of variables[1,2]. This entails a Fourier development in the vertical coordinate y, chosen so as to enforce the metallic wall boundary conditions on the upper and lower surfaces. Satisfaction of the boundary conditions on the vertical walls is a linear problem which has a solution except at certain frequencies, the frequencies of whispering gallery resonances. The pattern of resonances in the real part of the impedance is shown in Fig.1, for the parameters of the now defunct NSLS-VUV light source.

The spectrum from a Michelson interferometer at NSLS-VUV, reported in 2001[3,4], is shown in Fig.2. Measurements at lower frequencies, down to the shielding cutoff of CSR, were carried out by microwave techniques[5]. The comparison of measured frequencies with theory is shown in the Table 1; see Ref. 6 for details.

The vacuum chamber of the VUV ring approximated the case of the theoretical

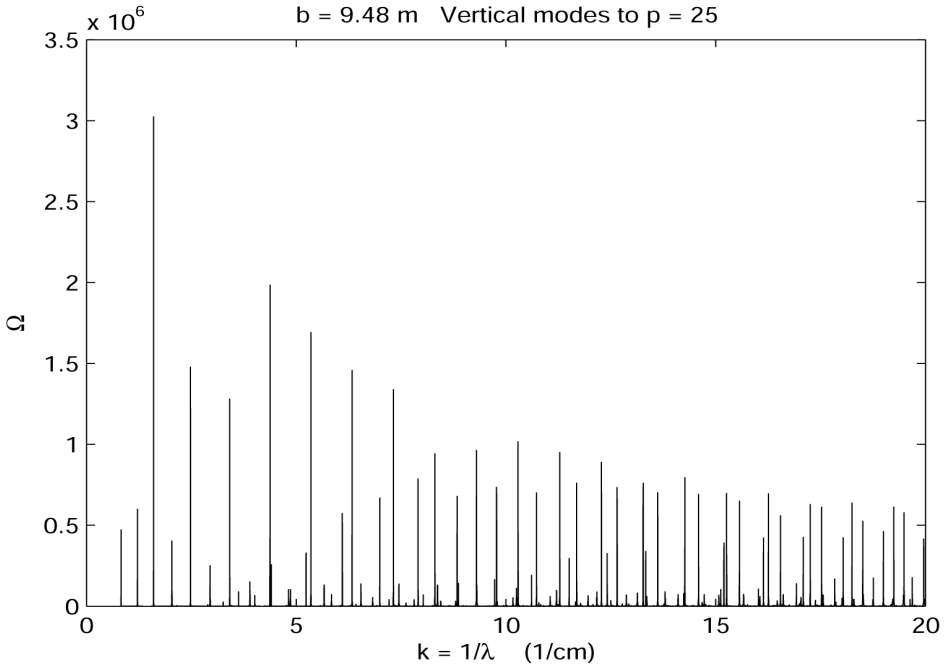

Fig. 1. ReZ(k) for parameters of VUV light source, vs. wave number $k = 1/\lambda$ in units of cm^{-1}.

Exp.	**Thy.**	**Exp.**	**Thy.**
0.80	0.827	6.10	6.31
0.93	—	7.25	7.32
1.32	1.21	9.00	8.32
1.57	1.60	10.0	9.29
2.10*	2.04	11.1	10.28
2.40	2.48	12.0	11.29
2.76*	2.94	12.8	12.33
3.10*	3.26	13.8	13.31
3.66*	3.62	15.0	14.3
3.88*	3.90	15.7-15.9	15.3
4.20	4.38	16.7	16.3
5.25	5.34	18.0	17.3
		18.8*	18.3

model to a good extent, except for the straight sections and the usual presence of small structures such as bellows. Assuming that the transitions to and from straight sections had a minor affect on gross radiation patterns, one can be encouraged by

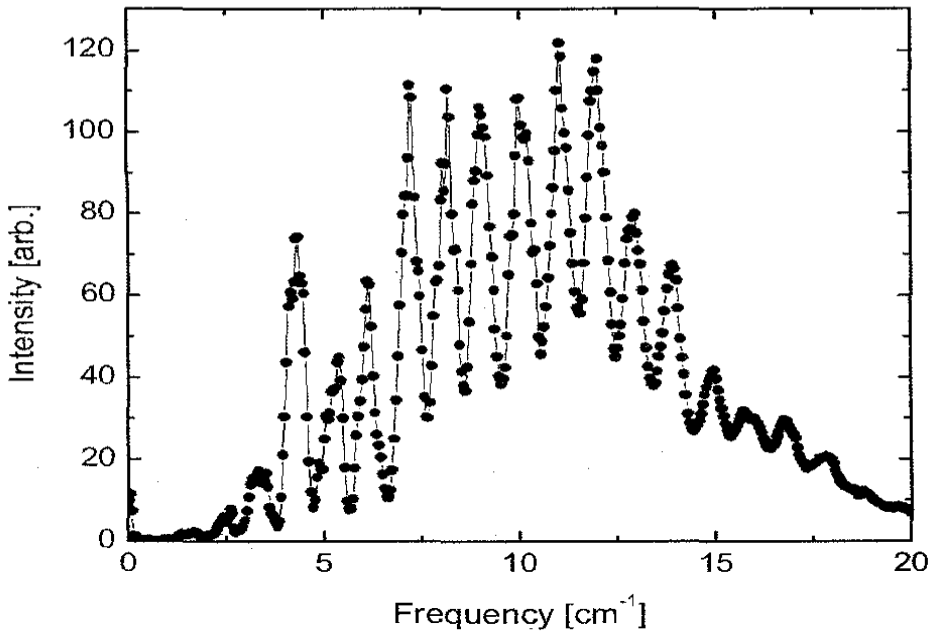

Fig. 2. Far IR spectrum measured at NSLS

the generally good agreement with theory in Table 1.

We should then go on to examine more recent observations. Precise measurements of CSR spectra in the far IR were carried out at the CLS[7] using a large interferometer, a Bruker IFS 125HR , capable of resolution down to $\Delta k = \Delta(1/\lambda) = 0.0008$ cm^{-1} . Spectra are typically in the range $6 - 15$ cm^{-1} or 0.18-0.45 THz, and have a form such as that displayed in Fig.3. The corresponding interferogram is shown in Fig.4. The position of the peaks was remarkably invariant with respect to changes in the machine setup (energy, bunch length, bucket filling pattern, CSR in bursting or continuous mode). Moreover, the pattern was the same over a span of years, during which equipment in the optical beam line was changed radically. This stability strongly suggests that the position of peaks is determined by the bend radius and the geometrical form of the vacuum chamber, as it would be in the simple toroidal model.

The average spacing of peaks is 0.074 cm^{-1}. To get such a small value from the toroidal model, the outer wall of the chamber would have to be 33 cm from the beam, much bigger than the average distance to the wall in the bends of the actual ring. This average distance to the wall is only vaguely defined, however, since in most of the bends there is a pumping slot in the wall, 1 cm high, which can allow some communication in short wavelengths with a large antechamber. There are two special bends in which the slotted wall is absent, and the beam has open

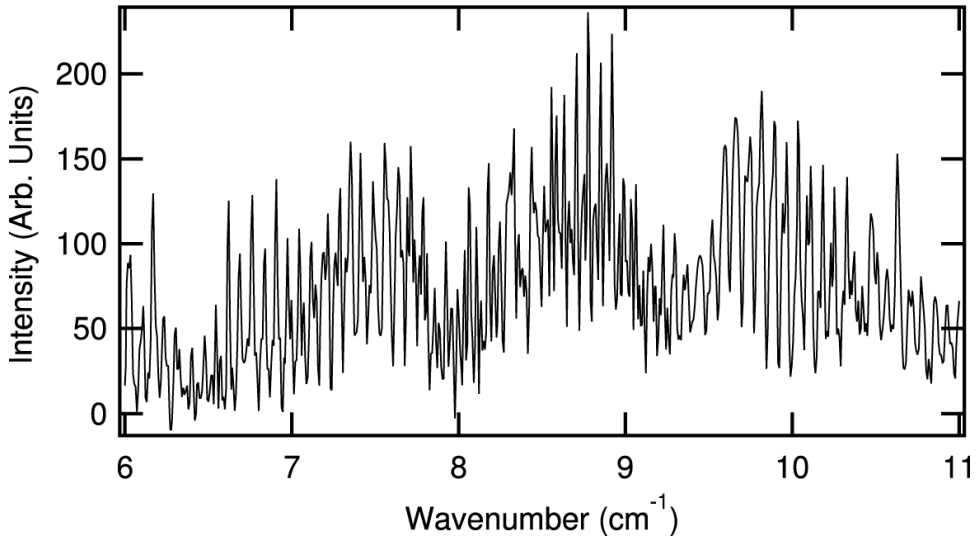

Fig. 3. Fourier transform of the interferogram. Peak spacing $\Delta k = \Delta\lambda^{-1} = 0.074$ cm^{-1}.

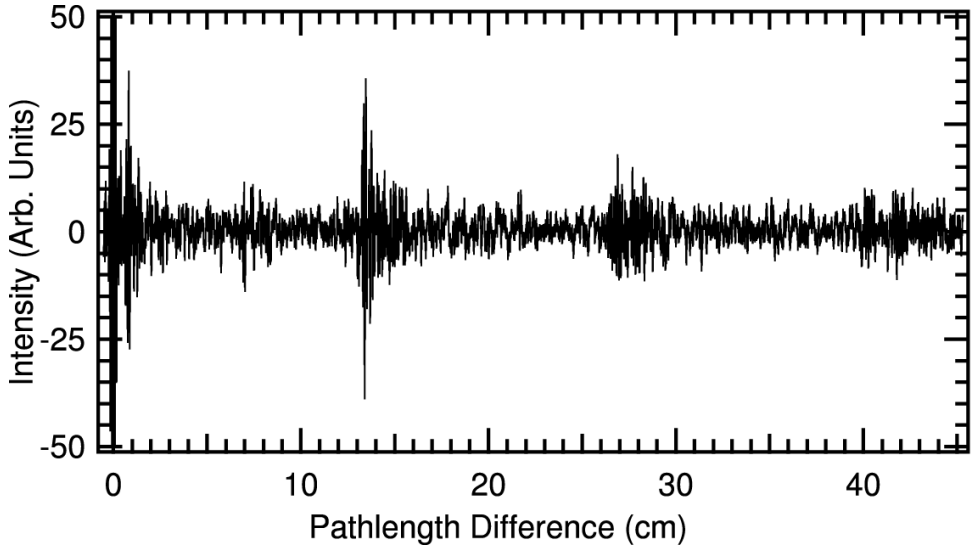

Fig. 4. Interferogram as a function of path length difference

communication with the full flared chamber as illustrated in Fig.5. The signal to the interferometer is picked up by the M1 mirror in such a bend, placed near the beam at the end of the 15° arc. The maximum excursion of the wall in the flared chamber is 33 cm from the beam, exactly the distance required in an unjustified application of the toroidal model. There is some reason to believe that this coincidence is not accidental, as I have found in a perturbative analytical model.

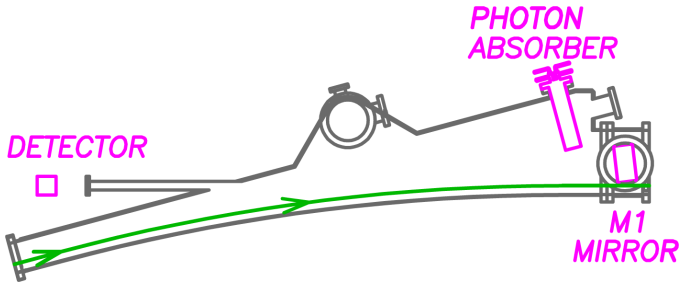

Fig. 5. Fluted vacuum chamber at the FIR dipole with bending radius $R = 7.143$ m and deflection angle $\theta = 15°$. The maximum excursion of the outer wall from the beam (——) is 33 cm.

It appears that detailed numerical modeling of fields in the flared chamber will be needed to understand the spectrum quantitatively. As a first step we have made some progress in analyzing the fields at lower frequencies, which are involved in a different kind of experiment at the CLS. Following a suggestion of Steven Kramer, a diode detector was installed behind an existing window (part of the original laser alignment system), so as to look upstream as shown in Fig.5. The detector catches backward propagating waves in the frequency range 30-110 GHz, being sensitive to horizontal or vertical polarization depending on its orientation.

Just by looking at oscilloscope traces of the detector signal, Jack Bergstrom contrived a picture of CSR waves developed in the bend and then reflected backward from the photon absorber, a copper bar filling a good part of the chamber cross section, and the metallic structure supporting the M1 mirror. He thought he could see not only the prompt pulse but also a pulse 12 cm behind, thus a long range wake field as predicted by the toroidal model. This was quite exciting, since a direct observation of these long range wakes had never been made before.

We therefore set about to simulate the experiment numerically, simplifying the geometry of the chamber by the model shown in Fig. 5.1 from D. Bizzozero's thesis[8]. Bizzozero integrated the six Maxwell curl equations in curvilinear coordinates, with time as the independent variable, after invoking a Fourier development in the vertical coordinate in such a way as to set the boundary conditions on the upper and lower surfaces. To discretize in the horizontal coordinate while meeting the boundary conditions on the vertical walls he applied the Discontinuous Galerkin (DG) Method, a sophisticated finite element method which shows good convergence in the presence of complicated boundaries. The source was a line charge with a Gaussian longitudinal charge density, $\sigma = 2$ mm. Simulation of the diode signal is based on the calculated values of E_x and E_y at the point where the tube leading to the diode meets the main chamber; the tube itself is not accounted for.

The upper graph in Fig.6 shows the simulated diode signal for horizontal polarization. The various peaks are correlated with experimental peaks in the red curve of the lower graph. The first two peaks, A and B, arise from reflections off the nearest structure, the photon absorber. The remaining peaks C-G come from the

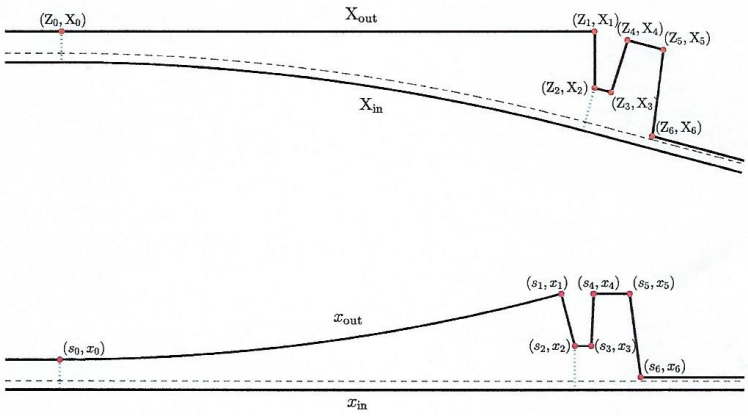

Figure 5.1: Physical laboratory frame (top) and Frenet-Serret transformed frame (bottom). The dashed line indicates the source's trajectory, the region between the dotted blue lines indicate where the curvature is non-zero, and the red dots indicate points where the boundary geometry transitions.

more distant mirror support structure, which is just a flat surface close to the beam in the model.

Of particular interest is peak B, which is 12 cm in spatial units behind the prompt pulse A. We view B as a wake field pulse, both expected in theory and seen indirectly in the interferogram of the other experiment. The pulse in the interferogram of Fig.4 is at 13.5 cm, essentially at the reciprocal of the peak spacing of 0.074 cm in its Fourier transform. The discrepancy between 12 cm and 13.5 cm is not necessarily detrimental to our interpretation, since the wake field is by definition dependent on the point of observation. Again, the peaks D, E, F, G are interpreted as successive wake pulses, with some correspondence to the interferogram. For a more detailed discussion see Ref. 7.

The DG simulation displayed complex and highly resolved local structures. Fig.7 shows the simulation of a leading pulse reflected from the photon absorber (left) and the later pulse from the M1 mirror assembly (right). The figure also shows the beginning of a long exit channel extending the computational domain to the right. It is so long that any wave reflected from its end does not come back to the main chamber during the time of computation. These computations were done on a GPU with the Matlab Parallel Toolbox.

The frequency spectrum of fields in this calculation cuts off at about 2.5 cm^{-1}, owing to the relatively long driving bunch of 2 mm. Thus we get no access to the domain of the spectrometer data of Fig.3. To go to high frequencies we could of course try to accommodate a shorter driving bunch through greater computer power,

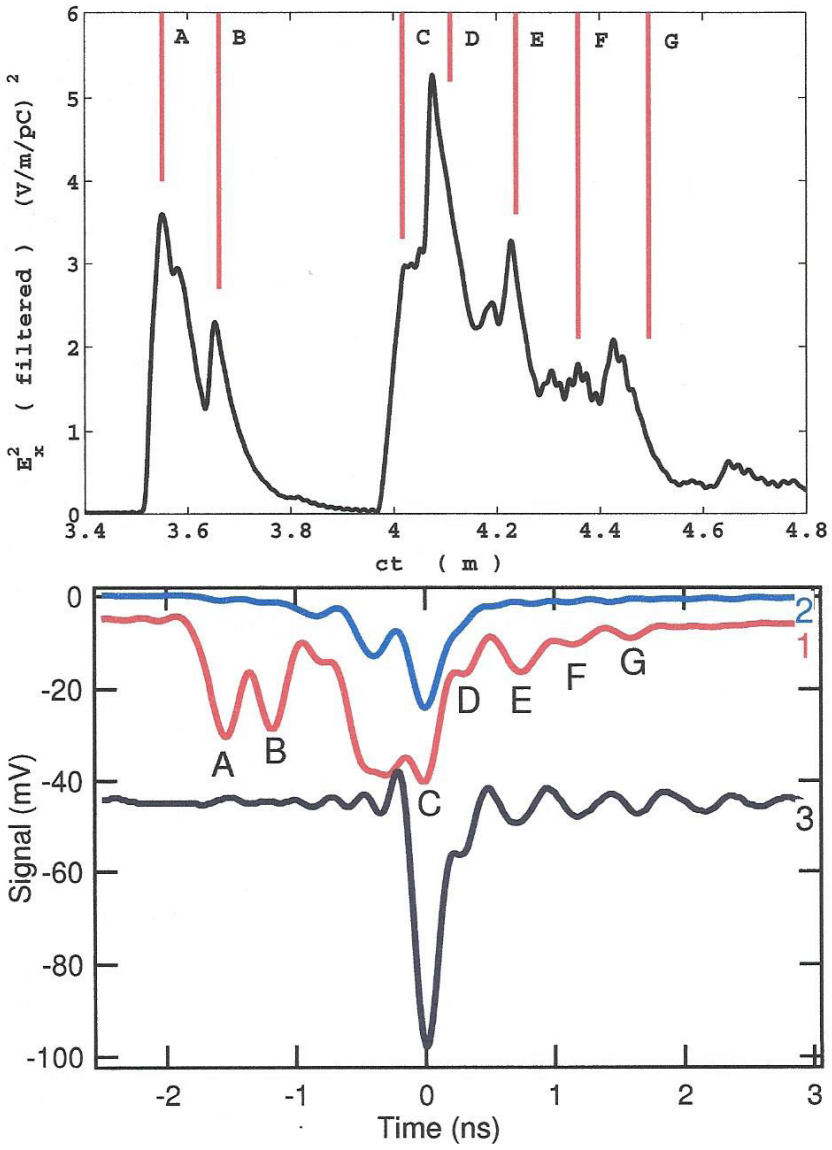

Fig. 6. Upper graph shows the simulated diode signal, with peaks correlated to experimental peaks A-G (red curve in lower graph)

but it seems more promising to abandon the time domain in favor of the frequency domain method developed in Ref. 9, but with important new improvements . In Ref. 9 we have already been able to treat CSR from a driving bunch of 0.01 mm with very modest computer demands, at least for a chamber with smooth walls.

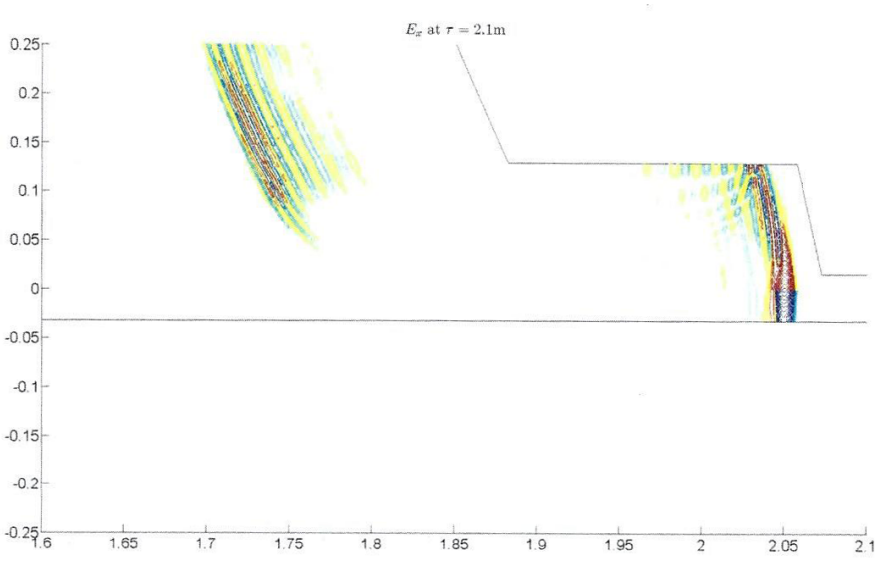

Fig. 7. Simulation of waves reflected from the photon absorber (left) and the M1 mirror support structure (right). Contour plots of E_x in the lowest vertical mode, at $t = 2.1$ m/c. The abscissa is s, the ordinate x, both in meters. The beam is at $x = 0$, the inner wall at $x = -0.032$ m.

2. A finite difference scheme in the frequency domain

The proposed method works in standard accelerator (Frenet-Serret) coordinates (s, x, y), with the reference trajectory in the plane $y = 0$ consisting of bends and straights in an arbitrary sequence. The vacuum chamber has top and bottom plates at $y = \pm g$, and inner and outer sidewalls at varying distances $x = x_-(s)$ and $x = x_+(s)$. It will be perfectly conducting, to start.

All field and charge/current components will represented as

$$F(s, x, y, t) = \sum_{p=0}^{\infty} \int_{-\infty}^{\infty} dk e^{ik(s-\beta ct)} \varphi_p(y) \hat{F}_p(s, x, k) \ . \tag{1}$$

The vertical Fourier mode φ_p is chosen to meet boundary conditions at $y = \pm g$; for instance for $F = H_y$ we have $\varphi_p = \sin(\pi p(y + g)/2g)$.

It is useful to think of (1) as the Fourier transform with respect to beam frame coordinate $z = s - \beta ct$ at fixed s. In another view it is merely the Fourier transform with respect to t at circular frequency $\omega = k\beta c$ with Fourier amplitude $\hat{G}_p(s, x, k) = \exp(iks)\hat{F}_p(s, x, k)$, hence an entirely general representation in which one chooses to separate the rapidly varying factor $\exp(iks)$ in the definition of the amplitude. The representation is general, but contains primarily right-moving waves if and only if $\hat{F}_p(s, x, k)$ is slowly varying in s.

All field components are expressed in terms of $\hat{E}_{yp}$ and $\hat{H}_{yp}$ and their derivatives

with respect to x and s; see Ref. 9, Eqs.(17)-(21). Moreover, $\hat{E}_{yp}$ and $\hat{H}_{yp}$ are the solutions of independent wave equations, not coupled even by boundary conditions (for perfect conductors). Within a bend of radius R, the field $u^E = \hat{E}_{yp}$ or $u^H = \hat{H}_{yp}$ satisfies

$$\begin{aligned}
&\frac{\partial^2 u}{\partial s^2} + 2ik\frac{\partial u}{\partial s} = \\
&-\left(\frac{x+R}{R}\right)^2\left[\frac{\partial^2 u}{\partial x^2} + \frac{1}{x+R}\frac{\partial u}{\partial x} + \left(\gamma_p^2 - \left(\frac{kR}{x+R}\right)^2\right)u - \hat{S}_p(s,x,k)\right] , \\
&\gamma_p^2 = k^2 - \alpha_p^2 , \quad \alpha_p = \pi p/2g .
\end{aligned} \tag{2}$$

where $\hat{S}_p$ is the appropriate source term for u^E or u^H, respectively.

One often invokes the Slowly Varying Amplitude Approximation (SVA), also known as the Paraxial Approximation. It amounts to throwing away the second derivative u_{ss}, under the assumption that

$$\|\frac{\partial^2 u}{\partial s^2}\| \ll 2k\|\frac{\partial u}{\partial s}\| , \tag{3}$$

where $\|\ \|$ is some appropriate norm. This does not make sense for $k \to 0$, but it only need be enforced for k above the "shielding threshold", the only region of interest for CSR. In the example studied in Ref. 9, which involved a vacuum chamber of constant width and a short bunch, we showed that (3) is valid. In earlier work by various authors the validity of SVA was simply assumed. Moreover, in unpublished work we showed that SVA was not bad in a chamber of mildly varying width, which yielded some limited insights on the effect of varying width. Even if there is a large variation in width, SVA can be valid as s varies until a strong backward wave is excited by some structure in the wall.

After dropping u_{ss} we can try a finite difference approximation to discretize (3). Let us first assume that the chamber has constant width, with inner and outer walls at $x = x_-$ and $x = x_+$, respectively. We define a mesh in x with N points,

$$x_j = x_- + (j-1)\Delta x , \quad \Delta x = (x_+ - x_-)/(N-1) , \quad j = 1, \cdots, N . \tag{4}$$

A simple scheme is derived by approximating the solution locally by a quadratic polynomial in x, at each $s = s_n = n\Delta s$. We write $u_j^n \approx u(s_n, x_j)$ for the approximate value at a mesh point, so that the quadratic formula is

$$u(x_j + p\Delta x) = \frac{1}{2}p(p-1)u_{j-1} + (1-p^2)u_j + \frac{1}{2}p(p+1)u_{j+1} . \tag{5}$$

Putting this into (2) and evaluating at mesh points we have

$$\begin{aligned}
&\frac{u_j^{n+1} - u_j^{n-1}}{2\Delta s} = \frac{i}{2k}\left(\frac{x_j+R}{R}\right)^2\left[\frac{u_{j+1}^n - 2u_j^n + u_{j-1}^n}{\Delta x^2} + \right. \\
&\left.\frac{1}{x_j+R}\frac{u_{j+1}^n - u_{j-1}^n}{2\Delta x} + \left(\gamma_p^2 - \left(\frac{kR}{x_j+R}\right)^2\right)u_j^n - \hat{S}_p(x_j, s_n, k)\right] , \\
&j = 2, \cdots, N-1 .
\end{aligned} \tag{6}$$

Here we have replaced $\partial u/\partial s$ by the central difference quotient; we shall comment on this choice presently.

For a first try the simplest choice for the charge and current densities is

$$\rho(s,x,y,t) = q\lambda(s-\beta ct)H(y)\delta(x)\ , \quad (J_s,J_x,J_y) = (\beta c\rho,0,0)\ ,$$
$$\int \lambda(s)ds = \int H(y)dy = 1\ , \tag{7}$$

namely, a line charge with arbitrary longitudinal and vertical densities, with total charge q. The corresponding sources for (2) are

$$\hat{S}_p^E = qZ_0\alpha_p c\hat{\lambda}(k)H_p\delta(x)\ , \quad \hat{S}_p^H = q\beta c\hat{\lambda}(k)H_p\big(\delta(x)/R+\delta'(x)\big)\ , \tag{8}$$

where Z_0 is the impedance of free space and $\hat{\lambda}$ and H_p are Fourier transforms of λ and H as defined in Ref. 9, Eq.(33). Owing to the presence of $\delta(x)$ and $\delta'(x)$ these sources cannot be represented numerically by their values on the x-grid, and (6) cannot be applied directly. To avoid this problem we change the dependent variable u to a new dependent variable, which satisfies a wave equation that is the same as (2) but has a smoother source denoted by $\tilde{S}_p$, amenable to representation by its values on the grid.

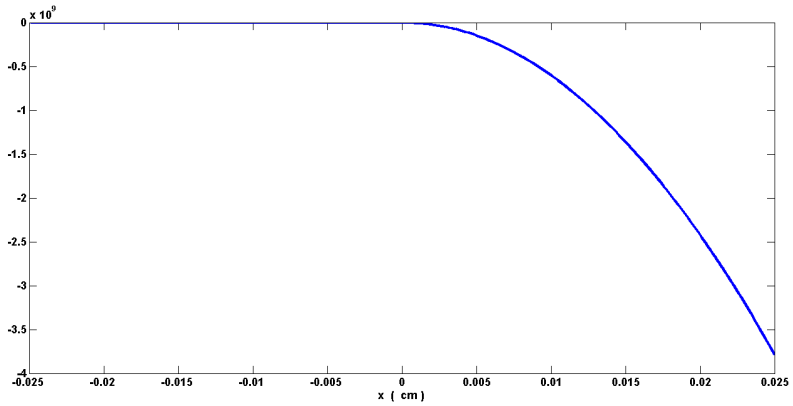

Fig. 8. The smooth effective source for the new dependent variable.

To see how this goes for $u = u^E$ we write $\hat{S}_p^E = c_1\delta(x)$ with c_1 being the coefficient given in (8). Then the expression in square brackets in (2) has the form

$$\Phi = u_x x + a(x)u_x + b(x)u - c_1\delta(x)\ . \tag{9}$$

We define a new dependent variable $u_1(x) = u(x) - \xi_1(x)$ where $\xi_1(x) = c_1 x\theta(x)$, with $\theta(x)$ being the unit step function (equal to 1 for $x \geq 0$, else equal to zero). Then Φ takes the form

$$\Phi = u_{1xx} + a(x)u_{1x} + b(x)u_1 - \sigma_1(x)\theta(x)\ , \quad \sigma_1(x) = -c_1(a(x)+xb(x))\ . \tag{10}$$

Hence u_1 satisfies the same wave equation as u, but with the piecewise continuous source $\sigma_1(x)\theta(x)$ replacing the delta function. Further transformations can make the effective source arbitrarily smooth[9]. The second transformation is $u_2(x) = u_1(x) - \xi_2(x)$, $\xi_2(x) = \sigma_1(0)x^2\theta(x)/2$. Then the source behaves as $x\theta(x)$ near $x = 0$ and has the graph shown in Fig.8. After trials with one, two, and three transformations, two emerges as a good choice. Putting $v = u_2$, we write the net result for the unknown function after two transformations as

$$v(x) = u(x) - \xi(x) \ . \tag{11}$$

The expressions for ξ and the corresponding smoothed sources $\tilde{S}_p$ are given in Ref. 9, Eqs. (54), (55). The boundary conditions are that $u^E(x_\pm) = 0$ and $\partial_x u^H(x_\pm) = 0$, hence the boundary conditions on v are

$$v^E(x_+) = -\xi^E(x_+) \ , \quad v^E(x_-) = 0 \ , \tag{12}$$

$$\partial_x v^H(x_+) = -\partial_x \xi(x_+) \ , \quad \partial_x v^H(x_-) = 0 \ . \tag{13}$$

To enforce the two conditions of (13) we make use of the quadratic interpolation (5), centered at x_2 for the inner wall and at x_{N-1} for the outer wall. Recalling (12), and taking the derivative of the interpolants to enforce (13), we have the boundary values as

$$v_1^E = 0 \ , \quad v_N^E = -\xi^E(x_+) \ , \tag{14}$$

$$v_1^H = \frac{4}{3}v_2^H - \frac{1}{3}v_3^H \ , \quad v_N^H = -\frac{2}{3}\Delta x \partial_x \xi^H(x_+) - \frac{1}{3}v_{N-2}^H + \frac{4}{3}v_{N-1}^H \ . \tag{15}$$

Returning now to (6), written for v rather than u with the appropriate smoothed

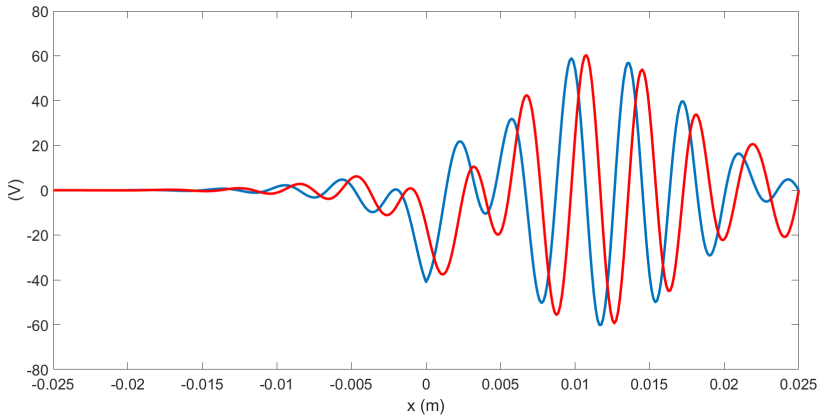

Fig. 9. Re $\hat{E}_{y1}(x)$ (blue) and Im $\hat{E}_{y1}(x)$ (red), $kR = 5 \cdot 10^5$.

source $\tilde{S}_p$, we substitute (14) and (15) for the boundary values on the right hand side. We then have $N-2$ equations to determine the $N-2$ interior values, assuming

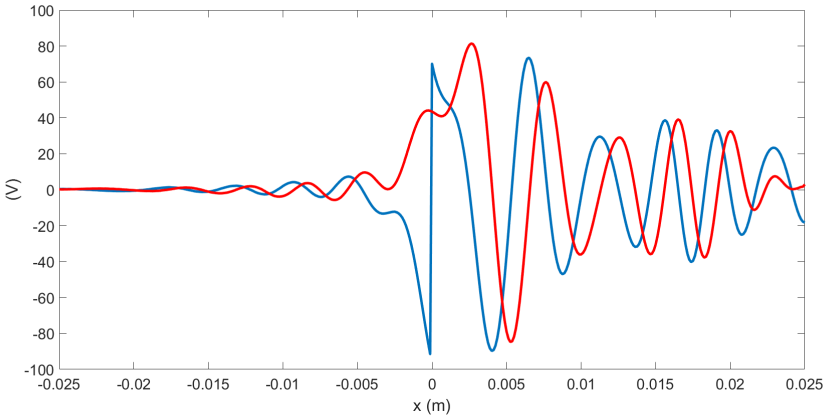

Fig. 10. Re $\hat{\mathrm{H}}_{\mathrm{y1}}(\mathrm{x})$ (blue) and Im $\hat{\mathrm{H}}_{\mathrm{y1}}(\mathrm{x})$ (red), $kR = 5 \cdot 10^5$.

a given initial condition v^0. To start the recursion on n we actually need v^1 as well as v^0, which we obtain by using Euler's method for the first step.

A code to realize the scheme is obviously short and simple. To illustrate we give an example already treated in Ref. 9 by a slightly more elaborate version of the present method, which used a 5-point interpolation rather than the 3-point. The parameters are for the final bend in the bunch compressor BC2 of LCSL-II: bend radius $R = 12.9$ m, bend angle $\theta = 0.0425$ rad, chamber width 5 cm, chamber height 2 cm. The charge is 100 pC, and the bunch is Gaussian in z and y with $\sigma_z = 10$ μm and $\sigma_y = 160$ μm. The initial condition is the steady state solution for the beam in an infinite straight pipe[9]. Fig.9 shows $\hat{E}_{y1}(x)$ and Fig.10 shows $\hat{H}_{y1}(x)$ (i.e., $p = 1$ vertical modes) at the end of the bend for $kR = 5 \cdot 10^5$, which means a frequency around the middle of the relevant range. Agreement of a new and simpler 3-point code with the older 5-point code of Ref. 9 is excellent, for the same Δx.

3. Chamber of varying width

To state the scheme most simply, suppose that only the outer wall position $x_+(s)$ varies with s; there is no special difficulty in allowing x_- to vary as well. Within a bend of radius R the boundary conditions at $x_+(s)$ are

$$v^E(x_+(s)) = -\xi^E(x_+(s)) \ , \tag{16}$$

$$\left[t_s(s)\partial_x u^H - \frac{t_x(s)}{1 + x/R}(iku^H + \partial_s v^H) \right]_{x=x_+(s)} = 0 \ , \tag{17}$$

where $\mathbf{t} = (t_s, t_x)$ is the unit tangent vector to the wall.

We define a fixed uniform mesh $\{x_i\}_{i=1}^N$ with $x^N > \max x_+(s)$, so that the mesh extends beyond the maximum excursion of the wall. Let $x_{i(n)}$ be the mesh point closest to $x_+(s_n)$, which may be inside or outside the wall. Then at $s = s_n$ the

right hand side of the differential system will be discretized as in (6) with just $i(n)$ points. Moreover, $v_{i(n)}$ will be given the value implied by the boundary condition and our basic interpolation (5). For instance, $v^E_{i(n)}$ is determined by (16) through the linear equation

$$v^E(x_+(s_n)) = \frac{1}{2}p(p-1)v^E_{i(n)-2} + (1-p^2)v^E_{i(n)-1} + \frac{1}{2}p(p+1)v^E_{i(n)} = -\xi^E(x_+(s_n)) \ , \qquad p = \big(x_+(s_n) - x_{i(n)-1}\big)/\Delta x \tag{18}$$

In a similar way, $v^H_{i(n)}$ is determined by (17) if we put $\partial_s v^H = ((v^H)^n - (v^H)^{n-1})/\Delta s$.

As n increases, $i(n)$ will occasionally increase or decrease by one unit. (We restrict Δs to be so small that it never changes by two units.) The code will be made to detect this one step before it happens, say at $n = n^* - 1$. If $i(n^*) = i(n) - 1$ we proceed to step n^*, in which the right hand side is now evaluated from v^n at only $i(n) - 1$ mesh points. If instead $i(n^*) = i(n) + 1$ we have to extrapolate the right hand side quadratically to define it at an additional mesh point $x_{i(n)+1}$, in preparation for step n^*.

This scheme was implemented for a mild wall perturbation, for example one period of a cosine curve with a small amplitude. We found that a field evaluated near the wall at its largest excursion had oscillations in its frequency spectrum with a shorter wavelength than those in the same field evaluated at $x = 0$. If this short wavelength pattern could somehow be reflected back to points near $x = 0$ by a more severe wall perturbation, we would have a qualitative explanation of the CLS spectrum, in which the wavelength at the M1 mirror seemed to be determined by the maximum excursion of the outer wall.

4. Larger steps in s through an implicit integration rule

A shortcoming of the method described is a limitation on the step size Δs, described by the Courant-Friedrichs-Lewy (CFL) stability condition. The CFL condition is that $r = \Delta s/(2k(\Delta x)^2)$ be sufficiently small; otherwise the iterates may grow without bound with increasing n. This is most restrictive at the minimum k, corresponding to the shielding threshold, such that $kR = 3.3 \cdot 10^4$ in the example above. With 400 cells in the x-mesh we found that instability set in at around $r = 0.23$, which implied about 30000 steps in s for stability at $k_{\min}$. In spite of this large number we were happy with the result since the method is still much faster than earlier CSR algorithms, even accounting for the cost of repeating the calculation for many values of k and p.

A well known way to overcome the CFL restriction is to apply an appropriate implicit integrator, in which v^{n+1} is not given explicitly in terms of v^n, but rather in terms of the solution of a certain nontrivial equation. If the solution of that equation is not too costly, an implicit method can have big advantages in speed by allowing a larger step size Δs.

Let us write the system of differential equations for the solution vector v, and

the equivalent Picard integral equation, as follows:

$$\frac{\partial v}{\partial s} = f(v,s)\ , \quad v(s+\Delta s) = v(s) + \int_s^{s+\Delta s} f(v(t),t)dt\ . \tag{19}$$

For small Δs the integral may be approximated by the trapezoidal rule,

$$\int_s^{s+\Delta s} f(v(t),t)dt \approx \frac{\Delta s}{2}\big(f(v(s),s) + f(v(s+\Delta s, s+\Delta s)\big)\ , \tag{20}$$

which suggests the Crank-Nicolson[10] or trapezoidal integrator,

$$\frac{v^{n+1}-v^n}{\Delta s} = \frac{1}{2}\big(f(v^n,s_n) + f(v^{n+1},s_{n+1})\big)\ . \tag{21}$$

5. Allowing a second derivative in s through an implicit integration rule

If we could restore the term $u_{ss} = \partial^2 u/\partial s^2$ that was dropped from (2) before discretization we would be dealing with the full Maxwell system, rather than the SVA (paraxial) approximation. A first try to do that is discouraging. If we merely add the lowest finite-difference form of $u_{ss}/2ik$ to the left side of (6) we get a system that is grossly unstable by experiment, using values of Δs that yielded stability without that term.

It did not occur to me that one might nevertheless get stability by means of an implicit rule, until I noticed a paper of Benedetti *et al.*[11] in which a method they called a Crank-Nicolson scheme included a term representing a second derivative. Their differential equation was different from ours, but I was nevertheless motivated to put the same term in our system. The favorable result is described in the sequel.

6. Marked acceleration of the algorithm by the trapezoidal method, with second derivative in s included

We now state the trapezoidal scheme (21) using the same 3-point interpolation in x that was used in (6). An important change, however, is that the forward difference quotient is used for $\partial v/\partial s$, as in (21), rather than the central difference of (6). Experiment showed that the central difference is detrimental in the trapezoidal method, which is perhaps not surprising in view of the derivation of (21). On the other hand, the central difference works very much better than the forward difference in the explicit method, in fact is essential for reasonable stability. By Taylor expansions the central difference gives a higher order approximation than the forward difference, but apparently that does not mean that it should always be used!

We state the equations, including a term for v_{ss}, making use of convenient

abbreviations:

$$\Delta(v_j^{n+1} - 2v_j^n + v_j^{n-1}) + v_j^{n+1} - v_j^n =$$
$$h_j(v_{j+1}^n - 2v_j^n + v_{j-1}^n + v_{j+1}^{n+1} - 2v_j^{n+1} + v_{j-1}^{n+1}) + k_j(v_{j+1}^n - v_{j-1}^n + v_{j+1}^{n+1} - v_{j-1}^{n+1}) +$$
$$l_j(v_j^n + v_j^{n+1}) - \sigma_j \Delta s \tilde{S}_j \ , \qquad j = 2, \cdots, N-1 \ , \tag{22}$$

where

$$\sigma_j = \frac{i}{2k}\left(\frac{x_i + R}{R}\right)^2 \ , \quad \Delta = \frac{1}{2ik\Delta s} \ ,$$
$$h_j = \frac{\sigma_j \Delta s}{2(\Delta x)^2} \ , \quad k_j = \frac{\sigma_j \Delta s}{4\Delta x(x_i + R)} \ , \quad l_j = \frac{\sigma_j \Delta s}{2}\left(\gamma_p^2 - \left(\frac{kR}{x_j + R}\right)^2\right) \ . \tag{23}$$

The linear equations for v^{n+1} have a tri-diagonal form, which we display as follows:

$$a_j v_{j-1}^{n+1} + b_j v_j^{n+1} + c_j v_{j+1}^{n+1} = d_j^n \ , \quad j = 2, \cdots, N-1 \ , \tag{24}$$

with

$$a_j = -h_j + k_j \ , \quad b_j = 1 + 2h_j - l_j + \Delta \ , \quad c_j = -h_j - k_j \ , \tag{25}$$
$$d_j^n = h_j(v_{j+1}^n - 2v_j^n + v_{j-1}^n) + k_j(v_{j+1}^n - v_{j-1}^n) + l_j v_j^n$$
$$+(1 + 2\Delta)v_j^n - \Delta v_j^{n-1} - \sigma_j \Delta s \tilde{S}_j \ . \tag{26}$$

One can think of different ways to enforce the boundary conditions. For a first try I have chosen to substitute in (24) the boundary values for *both* v^n and v^{n+1} as defined in (14) and (15). Another idea is to enforce the boundary condition only for v^{n+1}, which can be done in the Thomas method for solving the tri-diagonal system as described by Strikwerda[12] and others. This requires a generalization of Strikwerda's procedure in the case of v^H, employing the interpolants at the boundaries.

After substitution of boundary values the equations can still be written in the form (24), but with some redefinitions of the coefficients and right hand side. For $v = v^E$ the replacements are

$$a_2 \to 0 \ , \quad d_{N-1} \to d_{N-1} + c_{N-1}\xi^E(x_N) \ , \quad c_{N-1} \to 0 \ , \tag{27}$$

while for $v = v^H$ the replacements are

$$b_2 \to b_2 + \frac{4}{3}a_2 \ , \quad c_2 \to c_2 - \frac{1}{3}a_2 \ , \quad a_2 \to 0$$
$$a_{N-1} \to a_{N-1} - \frac{1}{3}c_{N-1} \ , \quad b_{N-1} \to b_{N-1} + \frac{4}{3}c_{N-1} \ ,$$
$$d_{N-1} \to d_{N-1} + \frac{2}{3}c_{N-1}\Delta x \partial_x \xi^H(x_N) \ , \quad c_{N-1} \to 0 \ . \tag{28}$$

In every case the values of v_1 and v_N that appear in d_2 and d_{N-1}, respectively, are to be as stated in (14) and (15).

We now have a redefined tri-diagonal system of the form (24), with $a_2 = c_{N-1} = 0$, which can be efficiently solved by the form of the Thomas algorithm given in Ref.

13. Taking first $\Delta = 0$ so as to omit the second derivative v_{ss}, we run the case of Figs. 9 and 10 and find curves that agree with those figures to graphical accuracy (save for a tiny discrepancy near $x = x_+$), and this is done with 100 steps in s rather than 30000. The cost per step is larger, but we nevertheless get an increase in speed by a factor of 70! In Ref. 9 we reported a time of 4.2 minutes on a single processor to compute the full wake field at the end of the bend, including the sum over values of k and p and some auxiliary calculations. With the new method this would be reduced by at least the factor of 70, to around 3.5 seconds. I believe that this is totally negligible compared to times with previous codes, and strengthens my prediction that charge/current construction and particle pushing would dominate if the method were applied to a macroparticle simulation. Compared to previous codes we both shorten the time for field calculation and improve the model of the vacuum chamber.

The next step is to restore the second derivative, again taking 100 steps. It is highly gratifying to find that the method is still stable. Moreover, the second derivative has hardly any effect on the solution, which is to be expected since we already know that the SVA (paraxial) approximation is good in the case of a smooth chamber. From the way that Δ occurs in the equations, it appears that the second derivative will have a minor effect if $|\Delta|$ is sufficiently small compared to 1; i.e., that Δs be sufficiently *large*. We are then called upon to see what happens with decreasing Δs. Indeed, we find that an instability sets in when Δs is too small, namely at about 150 steps at $k = k_{\min}$ (but proportionally more at the more relevant values of k well above the shielding threshold).

Without the second derivative it appears that the method is stable for "any" Δs, as is the case for the trapezoidal rule applied to simpler examples like the heat equation. There is a slow degradation in accuracy as Δs is increased, but more near the outer wall than in the region within the bunch, important for the beam dynamics.

7. Outlook

The most urgent task on the conceptual side is to allow a corrugated outer wall in the chamber, while including the second s-derivative. Superficially it would seem that the method would be stable for small Δ, irrespective of boundary conditions, but that might be too much to hope for. We have had some success in treating a mildly perturbed wall without the second derivative, so it seems probable that we could at least allow a stronger perturbation with the new method.

An immediate practical application, probably without the second derivative, would be to use our method as the field solver in a self-consistent macro-particle simulation of CSR in single-pass systems, such as a bunch compressor in an X-ray FEL. A sketch of how such a calculation would proceed is presented in Ref. 9, Sec. VII. The method of smoothing the effective source, presented here for the case of a line charge, can be generalized to handle a source with finite but narrow width, as

would be encountered in a realistic simulation; see Sec. III C in Ref. 9.

The present scheme, like earlier schemes with s as the independent variable, has not accounted for the periodicity of fields in a full ring, which is essential for global whispering gallery modes. It seems possible to adjust the initial condition to gain periodicity, except at certain frequencies, which would be the resonant frequencies. One can also think of an artificial periodicity over a distance less than a full turn, and that seems a good approach to study the resonance-like peaks in the CLS spectrum, which seem to be of local origin, not eigenmodes of the entire vacuum chamber. The artificial period could be somewhat longer than the length of the flared structure in the CLS.

A large part of the work of Ref. 9 was a study of energy deposited in resistive walls of the chamber. Our method makes it easy to find any component of any field at an arbitrary point in the chamber, once the basic solutions for $\hat{E}_{yp}$ and $\hat{H}_{yp}$ are known. Magnetic fields at the walls were used in a perturbative procedure to find the energy deposited. A non-perturbative treatment of the resistive wall will require some new ideas, which ought to be pursued.

8. Acknowledgment

I am saddened to report that Jack Bergstrom, my dear friend and collaborator over many years, left us on November 29, 2017. It will be hard to do without his probing questions, wide knowledge of the literature, and infectious enthusiasm. I also wish to thank David Bizzozero and Jim Ellison for much help in the early stages of this work. My work at SLAC was supported in part by the U.S. Department of Energy, Office of Science, Program in High Energy Physics, under Award No. DE-AC03-76SF00515.

References

1. R. Warnock and P. Morton, “Fields excited by a beam in a smooth toroidal chamber”, SLAC-PUB-4562 (1988), later published in Part. Accel. **25**, 113 (1990) but with different equation numbers.
2. K.-Y. Ng, “ Resonant impedance in a toroidal beam pipe”, Part. Accel. **25**, 153 (1990).
3. G. L. Carr, S. L. Kramer, N. Jisrawi, L. Mihaly, and D. Talbayev, “Two-beam interference of long wavelength synchrotron radiation”, Proc. 2001 Part. Accel. Conf., Chicago.
4. G. L. Carr, S. L. Kramer, J. B. Murphy, R. P. S. M. Lobo, and D. B. Tanner, “Observation of coherent synchrotron radiation from the NSLS VUV ring”, Nucl. Instr. Meth. Phys. Res. A **463**, 387 (2001).
5. S. L. Kramer and P. Podobedov, “Coherent microwave synchrotron radiation in the VUV ring”, Proc. Euro. Part. Accel. Conf. 2002, Paris; S. L. Kramer, “Direct observation of beam impedance above cutoff”, Phys. Rev. ST Accel. Beams **5**, 112001 (2002).
6. R. Warnock and J. Bergstrom, “Coherent radiation in whispering gallery modes”, Part. Accel. Conf. 2011 (PAC11), New York, paper WEP119; R. Warnock, “Electromagnetic Whispering Gallery Modes”, pp.113-135 in “Doing Physics: a Festschrift for

Thomas Erber", (IIT Press, Chicago, 2010). In Eq.11.31 of this paper the factor $2\pi R$ is on the wrong side of the equation.
7. B. E. Billinghurst, J. C. Bergstrom, C. Baribeau, T. Batten, L. Dallin, T. E. May, J. M. Vogt, W. A. Wurtz, R. Warnock, D. A. Bizzozero, and S. Kramer, "Observation of Wakefields and Resonances in Coherent Synchrotron Radiation", Phys. Rev. Lett. **114**, 204801 (2015).
8. D. Bizzozero, "Studies on Coherent Synchrotron Radiation with the Discontinuous Galerkin Method", Doctoral Dissertation, University of New Mexico, 2015.
9. R. L. Warnock and D. A. Bizzozero, "Efficient computation of coherent synchrotron radiation in a rectangular chamber", Phys. Rev. Accel. Beams **19**, 090705 (2016).
10. J. Crank and P. Nicolson, "A practical method for numerical evaluation of solutions of partial differential equations of heat-conduction type", Proc. Cambridge Phil. Soc., **43**, 53 (1947).
11. C. Benedetti, C. B. Schroeder, C. G. R. Geddes, E. Esarey, and W. P. Leemans, "An accurate and efficient laser-envelope solver for the modeling of laser-plasma accelerators", Eq.2, Plasma Phys. Control. Fusion **60**, 014002 (2018).
12. J. C. Strikwerda, "Finite difference schemes and partial differential equations", §3.5, (SIAM, Philadelphia, 2004).
13. http://en.wikipedia.org/wiki/Tridiagonal_matrix_algorithm